Regulation of cell fate in neurodevelopment and oligodendroglioma by the transcriptional repressor Capicua

Sheikh Tanveer Ahmad[1,2,3], Alexandra D. Rogers[2], Myra J. Chen[2,3], Rajiv Dixit[2,3,4], Lata Adnani[3,4], Luke S. Frankiw[2,5], Samuel O. Lawn[2,6], Michael D. Blough[2], Mana Alshehri[2], Wei Wu[2,7], Stephen M. Robbins[2], J. Gregory Cairncross[2], Carol Schuurmans[3,4], Jennifer A. Chan[1,2,3,*]

[1] Department of Pathology & Laboratory Medicine, University of Calgary, Calgary, Alberta, Canada
[2] Charbonneau Cancer Institute, University of Calgary, Calgary, Alberta, Canada
[3] Alberta Children's Hospital Research Institute, University of Calgary, Calgary, Alberta, Canada
[4] Sunnybrook Research Institute and the Department of Biochemistry, University of Toronto, Toronto, Ontario, Canada

Present addresses:
[5] Department of Biology & Bioengineering, California Institute of Technology, Pasadena, CA, USA
[6] Zymeworks, Vancouver, BC, Canada
[7] University of California, San Francisco, CA, USA

*Corresponding author:
Jennifer A. Chan
University of Calgary
Health Research and Innovation Centre, room 2A-A22
3330 Hospital Drive NW
Calgary, AB T2N 4N1
Canada
jawchan@ucalgary.ca

Keywords:
Capicua, CIC, oligodendroglioma, glioma, oligodendrocyte precursor cell, cell fate specification, gliogenesis, Etv5

ABSTRACT

Capicua (Cic) is a transcriptional repressor mutated in the brain cancer oligodendroglioma. Despite its cancer link, little is known of Cic's function in the brain. Here, we investigated the relationship between Cic expression and cell type specification in the brain. Cic is strongly expressed in astrocytic and neuronal lineage cells but is more weakly expressed in stem cells and oligodendroglial lineage cells. Examining a new conditional *Cic* knockout mouse, we show that forebrain-specific *Cic* deletion increases proliferation and self-renewal of neural stem cells. Furthermore, *Cic* loss biases neural stem cells toward oligodendroglial lineage selection, thereby expanding the pool of oligodendrocyte precursor cells (OPCs). These proliferation and lineage selection effects in the developing brain are dependent on de-repression of *Etv5*. In patient-derived oligodendroglioma cells, CIC re-expression or ETV5 blockade decreases proliferation and rescues the cells' capacity for differentiation. Our results identify Cic is an important regulator of cell fate in neurodevelopment and oligodendroglioma, and suggest that its loss contributes to oligodendroglioma by promoting proliferation and an OPC-like identity via overactivity of Ets factors.

INTRODUCTION

The identification of genes recurrently mutated in cancer often presents opportunities to uncover previously unappreciated mechanisms regulating normal development, and vice versa. The transcriptional repressor Capicua (*CIC*) has been identified as a likely tumour suppressor gene, as recurrent mutations in *CIC* and/or reduced expression of CIC have been identified in several cancer types, most notably in a subset of brain tumours. In the brain, *CIC* mutations are nearly exclusively found in oligodendrogliomas (ODGs) – glial tumors that most frequently occur in the frontal and temporal lobes and that are composed of cells resembling oligodendrocyte precursor cells (1, 2). Indeed, concurrent *IDH1/2* mutation, single-copy whole-arm losses of 1p and 19q, and mutation of the remaining

copy of *CIC* on chr 19q13 are highly characteristic of ODG and are not found in other cancer types (3-5). These associations suggest a unique relationship between CIC and the biology of glial / oligodendroglial cells.

Prior work in Drosophila and in mammalian cultured cells has shown that Cic is a transcriptional repressor downstream of receptor tyrosine kinase (RTK) signalling (6). Binding of Cic to the sequence T(G/C)AATG(G/A)A in enhancers and promoters leads to transcriptional repression of its target genes (7, 8). This default repression is relieved upon RTK signalling (6, 9-11), permitting transcription of targets – among which are *PEA3/ETS* transcription factors including *ETV1/4/5* (12). To date, however, little is known about the functional role of CIC in mammalian development or in the brain. Recent work by Yang et al. using *Cic* conditional knockout mice, reported that Cic loss can increase a population of proliferating Olig2+ cells in the brain, and that in a glioma model driven by *PDGFR* (analogous to a subset of RTK-driven human glioblastomas), loss of Cic potentiates glial tumorigenesis (13) – consistent with a role in glial biology. The mechanisms by which Cic loss affected those findings, however, remained undefined. Meanwhile, in the non-neoplastic context, Lu et al. recently showed that impairing the interaction of the Cic with the protein Ataxin 1 results in spectrum of neurobehavioral and neurocognitive phenotypes, as well as abnormal maturation and maintenance of populations of cortical neurons (14) – indicating a role for Cic in neuronal biology as well. Deciphering Cic's mechanisms of action as a neurodevelopmental regulator may shed light on these varied phenotypes resulting from Cic loss or abnormal function.

Here, we examine the temporal and spatial pattern of Cic expression in the mammalian cerebral cortex and white matter, and take a loss-of-function approach to examine its role in neuronal-glial identity determination. Our results reveal an important role for Cic in regulating lineage specification of neural stem cells during development – with loss favoring glial production at the expense of neuronal production. Furthermore, we show that these effects are mediated through Cic's regulation of the transcription factor Etv5. Our findings suggest that *CIC* mutation/loss contributes to ODG biology by

promoting aberrant proliferation / self-renewal and by stalling cells in an immature OPC-like state through de-repression of *ETV5*.

RESULTS

Cic expression levels are cell type- and stage-specific

As an initial step to investigating Cic's potential role in forebrain development and in oligodendroglioma, we examined its expression in several regions and developmental stages of the mouse brain. In bulk neocortical tissue, *Cic* transcripts and protein were detectable throughout development (data not shown). Closer examination of nuclear Cic protein expression by immunofluorescence staining, however, revealed marked differences in Cic expression between cell types.

Focusing first on the stem cell compartment, we assessed tissue from the dorsal telencephalon (the anlage of the neocortex) at embryonic day (E) E12. At this early neurogenic stage, non-lineage restricted neural stem cells are found in the ventricular zone (VZ) and can be identified not only by their spatial location but also by their expression of the transcription factor Sox2 (15). In Sox2+ VZ cells, Cic was localized predominantly in the cytoplasm, with weaker nuclear expression (Figure 1A). This distribution is consistent with the previous demonstration that growth factor/RTK signaling is locally elevated in the embryonic VZ (16, 17) and that Cic nuclear export is regulated by ERK-mediated Cic phosphorylation (6, 9-11). Pools of stem/progenitor cells are not limited to development, but also persist postnatally in the subventricular zone (SVZ) of the lateral ventricle and in the subgranular layer (SGL) of the hippocampal dentate gyrus (18, 19). In the SVZ and SGL of postnatal day (P) P56 mice, Cic was similarly weakly expressed in the Sox2+ compartment – in contrast to stronger expression in adjacent differentiated cells (Figure 1B,C). Thus, in both the embryonic and postnatal brain, neural stem cells are characterized by low levels of nuclear Cic.

As cells differentiated, Cic expression increased, albeit with notable differences between the levels detected in neuronal, astrocytic, and oligodendrocytic cell lineages. In the adult (P56) cortex, NeuN+ neurons displayed the strongest expression of Cic, with a distribution that was distinctly nuclear (Figure 1I). The increase in nuclear Cic within the neuronal lineage was detectable during the process of embryonic neurogenesis, with a modest increase detected as cells transitioned from Sox2+ stem cells to Tbr2+ neuronal intermediate progenitors, and a more marked elevation in Tbr1+ post-mitotic neurons in the intermediate zone and cortical plate – where nuclear Cic levels approached those of mature neurons in the adult cortex (Figure 1G,H,I, J). In GFAP+ or Aldh1+ astrocytes in the cortex and underlying white matter, levels of nuclear Cic also increased relative to Sox2+ cells (Figure 1D,J; Supplemental Figure S1A).

The lowest levels of nuclear Cic were found in oligodendroglial lineage cells. Olig2 is a bHLH transcription factor that is expressed in cells at or before oligodendrocyte specification and continues to be present throughout oligodendroglial lineage development (20, 21). Within the Olig2+ population, the subset of Pdgfra+ cells indicative of oligodendrocyte precursor cells (OPCs) had the lowest levels of all, with a modest increase as cells transitioned from Pdgfra+ OPCs to CNPase+ immature oligodendrocytes (Figure 1E, F, J) and later to mature myelinating CC1+ oligodendrocytes (Supplemental Figure S1B). Overall, the mean integrated nuclear signal intensity for Cic was significantly lower in Sox2+ and Pdgfra+ cells than in including NeuN+ cells ($p < 0.0001$), Tbr1+ cells ($p < 0.0001$), or Gfap+ cells ($p < 0.01$) (Figure 1J and Suppl S1).

This pattern of higher nuclear Cic expression in neurons and astrocytes and lower levels in stem cells and oligodendrocytes (particularly OPCs), raised the possibility that nuclear CIC bound to its target genes may repress stem- and/or oligodendroglial-promoting programs to influence cell fate.

Cic-deficiency results in increased glial populations and decreased neuronal populations during forebrain development

To directly test whether Cic could regulate stemness or cell fate decisions, we performed a series of loss-of-function studies. Cic contains several critical domains including an HMG-box and a C-terminal C1 domain that together bind to DNA, and a C-terminal Gro-L domain that mediates protein-protein interactions (10, 22-25). We generated *Cic* conditional knockout mice in which exons 2-11 of *Cic* gene were flanked by loxP sites, with the floxed region containing all exons encoding the HMG box. Upon introduction of Cre, exons 2-11 are excised and the remaining exons 12-20 are frameshifted, thus ablating the HMG box, C1 domain, and Gro-L domain (Figure 2A). We used these animals for in vivo studies as well as to generate cell lines with which we could further study lineage selection and differentiation.

By crossing *Cic*-floxed mice to *Foxg1-Cre* mice (in which *Cre* is expressed throughout the forebrain by E10.5 (26)), we generated mice deficient in CIC in the embryonic telencephalon and the subsequent postnatal cerebrum (Figure 2A,B). $Cic^{Fl/Fl}$;$FoxG1^{Cre/+}$ (CIC forebrain-null) animals were born in approximate Mendelian ratios and were grossly indistinguishable at birth. They failed to thrive postnatally, however, becoming visible runts by approximately postnatal day 7, and were uniformly lethal by P21-22 (Figure S2B) when they did not survive past weaning. Gross examination of brains at P21 showed that although Cic-null brains were smaller overall than littermate controls, all major forebrain structures were present (Figure 2C). Cursory light microscopic exam also showed the presence of laminated cortex and the overall development of normal anatomic structures such as the hippocampi (Figure S2A).

Closer evaluation of P21 cortices, however, revealed a shift in cell populations, with comparatively fewer neurons and comparatively increased oligodendroglial cells and astrocytes present in Cic-null cortices compared to controls (Fig 2D,D',E,E'). In Cic-null cortices, NeuN+ cells comprised 76.6±2.5% of total cells; whereas in controls that were either CIC-floxed but without Cre ($Cic^{Fl/Fl}$; $FoxG1^{+/+}$) or that were heterozygous for Cic loss ($Cic^{Fl/+}$; $FoxG1^{Cre/+}$), NeuN+ cells comprised 82.04±2.78% of the total cells

(n=5, p<0.05). In contrast, a moderate increase was observed in Gfap+ cells in knockouts relative to wild-type cortices (12.46±1.49 CIC-null *vs.* 9.61±1.39 Cic-wt; n=5, p<0.05). The greatest change, however, was observed in the number of oligodendroglial lineage cells present; Olig2+ cells were increased in Cic-null cortices compared to controls (10.83±1.47% *vs.* 4.99±0.87%, in Cic-null vs control, respectively; n=5, p=0.0001) as were Sox10+ cells (11.72±1.83% *vs.* 7.43±0.94%; n=5, p=0.0001).

One possibility that could explain such a skewing of cell populations could be that there was increased death in a particular population. However we found no evidence of increased apoptosis as indicated by activated caspase-3 in the knockout brains (Figure S2E). Other possibilities, were that Cic loss could be increasing proliferation and/or affecting lineage selection – possibilities that we continued to explore by turning our attention to the neurogenic period.

CIC increases proliferation of neural stem/progenitor cells

Others have recently reported proliferative gains upon loss of Cic (13), and we too found evidence of increased proliferation. By electroporating pCIG2-Cre (or control pCIG2 empty vector) into $Cic^{Fl/Fl}$ embryos, we could study the effects of Cic loss in a discrete population of GFP+ targeted cells (Figure 3A). Cre electroporation into E13 VZ (early to mid-neurogenesis) resulted increased proliferation as determined by EdU incorporation and increased numbers of Sox2 positive cells among the targeted cell population within 48 hours (Figure 3B). EdU+ cells increased by 2.6-fold in cre-electroporated cells compared to controls (pCIG2-Cre; 9.99±0.92%, n=4, *vs.* pCIG2-Empty; 3.77±0.81%, n=5, p<0.0001)(Figure 4A,A'). Among GFP+ cells, the fraction expressing Sox2 in cre-electroporated brains was 5.48±1.01%, compared to 11.09±1.10% control-electroporated brains (n=5 and n=4, respectively; p<0.05) (Figure 3B,B'). Consistent with the increased proliferation of neural stem cells in vivo upon CIC deletion, cultured cell experiments also showed increased proliferation and self-renewal of CIC null NSCs in vitro. *Cic* null and control NSC lines were derived from E15 *Cic*-floxed cells transfected ex-vivo with Cre or control plasmids (Figure 4B). When maintained in serum-free NSC proliferation media, Cic-

null and control cells both maintained expression of stem cell markers such as Sox2 and the intermediate filament protein nestin (Figure 5A,B). When Cic-null and control cells were seeded at equal numbers and grown in NSC proliferation media, Cic-null cells displayed a 3-fold increase in cell numbers relative to controls by 3 days post-plating (Cic-null; 2.90±0.44, n=4, *vs.* Cic-wt; 0.98±0.12, n=3, $p<0.01$) (Figure 4C). These data were corroborated by Alamar blue assay (Figure S2A), Ki-67 immunostaining (Figure 4D) and cell cycle analysis (Figure 4E), all of which showed increased proliferation in Cic-null cultures than in controls. There were no significant differences in the numbers of dead cells (Figure S2C), indicating that the differences in viable cell numbers for Cic-null cells was due to their higher proliferative rates, rather than reduced viability. Together, these data support that Cic is a strong negative regulator of proliferation in forebrain NSCs.

The proliferative increase upon *Cic* deletion was accompanied by increased self-renewal, as determined by a clonogenic assay (Figure 4F). In this assay, after plating equal numbers of dissociated cells in semi-solid media, a higher number of spheres indicates higher number of self-renewing cells in the initial population, whereas sphere volume is a more general indicator of proliferation that includes the influence of factors such as cell cycle kinetics, modes of cell division, and the fraction of cells remaining in or exiting the cell cycle. Both Cic-null and control NSCs were able to self-renew, generating clonal spheres from individual cells (Figure 4F). Cic-null NSCs, however, generated higher sphere counts than control NSCs (9-fold increase in sphere generation over control; $p < 0.0001$, n= 3)(Figure 4F,4F'). Spheres were also larger for Cic-null cells compared to control (10.1-fold increase in calculated μm^3 over control; n=3, $p<0.0001$)(Figure 4F,F''). Thus, Cic loss confers not only higher proliferation potential but higher self-renewal capacity in NSCs, at least when cells are in an environment promoting neural stem cell proliferation. While the proliferative effects of Cic deficiency in NSCs seem clear, what was intriguing were additional changes in observed in Cic-null cells/brains that suggested a lineage selection bias in NSCs.

***Cic* ablation increases expression of the glial / oligodendrocyte lineage determinants Sox9 and Olig2 in NSCs**

While there was no difference in the expression of Sox2 and Nestin between Cic-null and control NSCs, as expected, expression of other glial / oligodendroglial transcription factors was aberrantly increased. Sox9 is an HMG-box transcription factor present in stem cells, glioblasts, and later glial cells but not in neuronal precursors or neurons, and its expression is critical in driving the gliogenic program (27, 28). The fraction of GFP+ cells expressing Sox9 was 2.5-fold that observed in controls (pCIG2-Cre; 15.97±1.69% *vs.* pCIG2-Empty; 6.37±1.60%, n=4 $p<0.05$) (Figure 3C,C'). Consistent with the increased fraction of cells expressing glial precursor markers at E13, following the targeted cells to E18 (5 days post-electroporation) revealed that a greater number of Cre-electroporated cells subsequently became Aldh1+ astrocytes (pCIG2-Cre; 3.65±1.31%, n=5, *vs.* p-CIG2-Empty; 1.664±0.91%, n=6, $p<0.05$)(Figure 3E,E') or Pdgfra+ OPCs (pCIG2-Cre 13.29±1.04%, *vs.* p-CIG2-Empty 5.87±2.54%; n=4, $p<0.01$) (Figure 3C,C'). In contrast, fewer became Tbr1+ early-born/deep-layer neurons (pCIG2-Cre 1.66±0.91% *vs.* pCIG2-Empty 4.62±1.04%; n=5, $p<0.01$) (Figure 3D,D'). As there was no observed difference in cell death between Cre- and control-electroporated populations (Figure S2D,D'), the findings suggest that that Cic likely has a role in cell lineage specification in neural stem cells. These findings were echoed in the expression of stem and neural lineage markers in cultured cells. As expected, when cells were grown in NSC media, both Cic-null and control cells equally expressed Nestin, and were largely devoid of the astrocytic marker Gfap or the pan-neuronal cell marker βIII-Tubulin as detected by Tuj1 (labels early and late stage neurons)(Figure 5A,B). There, was, however a marked increase in Sox9 expression in Cic-null cultures compared to controls (Cic-null 37.4±3.6% *vs.* Cic-wt 12.3±2.1%; n=3, $p < 0.01$)(Figure 5A,B). Olig2 was similarly elevated in Cic-null cells (Cic-null 29.8±2.9% *vs.* Cic-wt 14.2±3.5% in controls; n=3, $p<0.01$) (Figure 5A-C). The increased Sox9 and Olig2 in Cic-null cells suggest that Cic deficiency sets an intrinsic foundation for pro-oligodendroglial programs very early in the neural cellular hierarchy.

Cic deficient cells are less responsive to extrinsic cues for neuronal and astrocytic differentiation, and are biased to the oligodendroglial lineage

We then asked whether exposure to exogenous factors could overcome the pro-oligodendroglial priming we observed in Cic-null NSCs. We challenged Cic-null and control NSCs with 10 days exposure to lineage-promoting culture conditions and then analyzed them for protein expression and morphology. Neuronal differentiation was induced by culturing cells with B27 and cAMP. After 10 days, Cic-null cultures had a lower percentage of bIII-Tub+ neurons compared to control cultures (CIC-null 24.0±9.2% *vs.* CIC-wt 67.8±8.5%, respectively; n=3, $p<0.01$) – a finding corroborated by western blotting (Figure 5C,C'). Astrocytic differentiation was induced by culturing cells in 1% FBS and N2. *Cic* null cultures had lower expression of Gfap (29.1±5.5% *vs.* Cic-wt 68.2±10.4%; n=3, $p <0.01$)(Figure 5D,D'). Furthermore, Cic-wildtype cells displayed more developed cell processes in their bIII-Tub+ or GFAP+ populations than did their Cic-null counterparts (Figures 5C,D). Oligodendroglial differentiation was induced by culturing cells in media with B27 and tri-iodo-thyronine. Staining of the differentiated cells for Olig2 revealed higher numbers of Olig2+ cells in Cic-null cultures compared to control (Cic-null 68.0±1.6% *vs.* Cic-wt 54.1±0.9%; n=3, $p < 0.01$) as well as increased Olig2 in western blots (Figure 5E,E'). These data support that Cic-null NSCs are biased away from neuronal and astrocytic specification and toward oligodendrocytic specification – a bias that cannot be overcome by extrinsic cues.

***Cic* deficient cells fail to progress normally through the OPC state**

Once progenitors commit to a lineage, they must differentiate to give rise to mature cells. Oligodendrocyte differentiation is a continuum characterized by the sequential expression of several markers (29). Olig2 overlaps with the stem cell compartment but is present throughout the oligodendrocyte lineage. Sox10 is induced immediately after oligodendroglial specification and also remains present through the mature stage (30, 31). In addition to Olig2 and Sox10 as pan-oligodendrocytic lineage markers, several stage-specific markers are known. First, OPCs additionally

express Pdgfra and NG2. Subsequently, immature or pre-myelinating oligodendrocytes begin to express O4 and CNPase. Finally, myelinating oligodendrocytes produce a variety of myelin-associated proteins such as myelin basic protein (MBP), myelin associated glycoprotein, and myelin proteolipid protein. We asked whether *Cic* modulates the ability of cells to proceed normally through differentiation once the oligodendroglial lineage is specified. By assessing Olig2, Sox10, PDGFRa, CNPase and MBP expression, we characterized progress through differentiation in the absence and presence of *Cic*.

When NSCs were cultured in oligodendroglial differentiating conditions for 10 days, Cic-null cells had a greater percentage of Olig2+ Pdgfra+ cells than in Cic-wildtype cultures (Cic-null 68.8±2.4% vs. Cic-wt 39.3±3.8%; n=5, $p < 0.0001$)(Figure 4E,H). Conversely the percentage of Olig2+MBP+ cells was decreased in Cic-null cultures compared to controls (Cic-null 2.1±1.5% vs. Cic-wt 8.2±3.0%; n=5, $p < 0.0001$)(Figure 4E,H). Furthermore, of the few Cic-null Olig2+MBP+ cells that were present, process formation was rudimentary compared to Cic-wildtype cells (Figure 4E).

Findings consistent with an oligodendrocyte maturation defect were also observed in vivo. In CIC-null brains, although Olig2+Pdgfra+ OPCs were increased compared to controls (44.53±3.80% of cells were Olig2+Pdgfra+ in $CIC^{Fl/Fl}$;$FoxG1^{Cre/+}$ *vs.* 28.20±1.95% in controls; $p<0.01$), CNPase+ cells were comparatively decreased (*$CIC^{Fl/Fl}$;$FoxG1^{Cre/+}$* 38.0±9.78% *vs.* Control 72.92±3.88%; n=5, $p<0.0001$) (Figure 2E,E'). Furthermore, Mbp expression in the white matter was decreased in *$Cic^{Fl/Fl}$;$FoxG1^{Cre/+}$* brains compared to controls (n=6, $p < 0.01$). Together, these data support that in the context of CIC deficiency, despite an increased proliferation of NSCs, an NSC bias to oligodendrocyte specification, and an increased in OPCs; the generation of mature myelinating oligodendrocytes is decreased.

Ets factors are transcriptional repressive targets of Cic in the forebrain

As Cic is a known transcriptional repressor, one mechanism for our findings is that Cic loss de-represses specific pro-glial / pro-oligodendroglial transcription factors. In this respect, *Etv* genes, which encode

Ets-domain transcription factors, are candidate target genes of interest. *Etv* genes (Etv 1, 4, 5) have been identified as direct targets of Cic in various mammalian cells and tissues (12, 32), and ETV genes are overexpressed in ODGs (33). Furthermore, previous studies have documented Cic occupancy at the *Etv5* promoter in cerebellar tissue (34).

To determine whether de-repression of *Etv* genes could be responsible for the phenotype we see from Cic loss, we measured *Etv1*, *Etv4* and *Etv5* transcript levels in cultured Cic-null and control cells by NanoString after 2 days of culture in differentiating conditions. We found that *Etv5* increased ~37 fold and *Etv4* transcripts were increased ~19 fold in Cic-null cells versus control cells whereas *Etv1* transcripts were unchanged (Figure 6A). Examination of protein levels in the cultured cells by western blotting also confirmed marked increases in levels of Etv4 and Etv5 in Cic-null cells (Figure 6B). Although both *Etv4* and *Etv5* were both de-repressed upon Cic loss, because of the comparatively greater levels of Etv5 relative to Etv4, as well as previous studies suggesting a role for *Etv5* in mediating glial and oligodendroglial fate decisions (35), we focused our further functional studies on this specific Ets-domain transcription factor.

In line with previous studies showing that *Etv5* could be a target of Cic, we confirmed that in forebrain tissue, *Etv5* showed evidence of promoter occupancy by Cic via ChIP-PCR (Figure 6C). Furthermore, in vivo electroporation of *Cic* shRNA into the telencephalic VZ resulted in upregulation of *Etv5* transcript levels in the electroporated patch within 48 hours, supporting the notion that it is indeed a functional target of Cic in vivo (Figure 6D). Similarly, examination of *Cic*-floxed, Cre-electroporated brains showed an increase in Etv5 protein (Figure 6E). Consistent with the repression of Etv5 by Cic, the levels of Etv5 and Cic in normal brain generally showed an inverse relationship; stem cells (Sox2+) and OPCs (Pdgfra+), which have the lowest levels of nuclear Cic (Figure 1) express the highest levels of Etv5. Cells such as Gfap+ or CNPase+ cells that had higher Cic expression conversely had lower levels of Etv5 (Figure 6F-K, Figure S4B). A similar pattern was observed for Etv4 protein expression in tissues (Figure S4A-B, D-D'), but its overall levels were lower than for Etv5.

De-repression of *Etv5* mediates the proliferative OPC phenotype of *Cic* deficient cells

Finally, to determine whether the increased proliferation and OPC bias that we observed in Cic-null cells was mediated by Etv5, we overexpressed wild-type *Etv5* or performed epistasis experiments introducing a dominant negative form (*DNETV5*) in which *Etv5* was fused to the *Engrailed* transcriptional repressor domain. Many of the differentiation/fate sequelae observed with *Cic* loss were recapitulated by *Etv5* overexpression. Electroporation of wild-type *Etv5* was sufficient to increase proliferation in vivo (Figure 7D, D', S5A). Similarly, wild-type *Etv5* overexpression acutely increased proliferation of cultured NSCs (Figure 7F, S5C'). Conversely, proliferation of *Cic*-deficient cultured NSCs returned to control levels after either introduction of *DNETV5* or knockdown by *Etv5* siRNA (Figure 7F-G, Suppl Figure S5). In vivo, the increased proliferation of the *Cic*-deleted cells returned to control levels (Figure 7E, E' compared to 7D,D'; Figure S5). In culture, Olig2+ cells as well as Olig2+Pdgfra+ OPCs returned to control levels (44.6±12.0% in Cic^{null};*DNETV5* cells *vs.* 62.5±14.6% in Cic^{null} cells; n=3, $p<0.05$). The percentage of cells expressing MBP also showed a substantial although partial rescue (5.3±2.9% in Cic^{null};*DNETV5* cells *vs.* 2.1±1.5% in Cic^{null} cells; n=3, $p < 0.05$) (Figure 7C-C'). Thus, Etv5 is both necessary and sufficient for inducing the proliferation and cell fate bias effects downstream of CIC loss.

We then used 2 oligodendroglioma cell lines, BT54 and BT88, to further investigate the importance of *CIC* mutation/loss in human disease. Both of these patient-derived lines harbour the characteristic whole-arm chromosome 1p and 19q losses that are diagnostic of ODG (36). As well, BT54 harbours a splice acceptor site mutation in the remaining *CIC* exon 6 while BT88 harbours a missense mutation in the remaining *CIC* exon 20 (3). In both BT54 and BT88, either stable re-expression of wildtype CIC or stable expression of *DNETV5* significantly reduced proliferation as measured by EdU incorporation (Figure 8A,A',C). Sphere-forming ability was also decreased by *CIC* expression or by introduction of *DNETV5* (Figure 8B,B',B'',D,E). These results were also confirmed by transient siRNA experiments to knock down Etv5 in BT-88 cells that also showed decreased proliferation and sphere formation (data

not shown). Consistent with an ongoing requirement CIC loss or Etv5 expression for proliferation and self-renewal in ODG, in vivo tumorigenicity of BT88 cells was markedly reduced by stable expression of either wildtype *CIC* or *DNETV5* (Figure 9). Thus, in cells that are already transformed to ODG, CIC loss remains important to sustain the proliferative phenotype of the cells – a phenotype that is large mediated through Etv5.

A similar finding was observed when we assessed the ODG cell lines' ability to differentiate in response to oligodendrocyte differentiation conditions. Both CIC re-expression and DNETV5 similarly resulted in increased expression of CNPase in the ODG cells compared to BT-88 control cells, indicating at least some improvement in capacity for the tumour cells to differentiate and mature (Figure 8F,F' bottom row panels). This is consistent with CIC loss and resulting Etv5 de-repression being important mechanisms also for maintaining the OPC-like phenotype of ODG. Interestingly, however, effects on neuronal and astrocytic differentiation, were mixed (Figure 8F,F' top and middle row panels). Cic re-expression resulted increased the ability of cells to respond to extrinsic neuronal differentiation cues by increasing expressing bIII-Tubulin (TUJ1) and extending neurites; however this was not phenocopied by DNETV5. With respect to expression of GFAP in response to astrocytic differentiation cues, no significant differences were detected with either CIC re-expression or DNETV5 introduction compared to BT-88 control. The latter data suggest that other genetic (or epigenetic) alterations may be more central to driving or maintaining some specific aspects of the cells' phenotypes, at least in our cultured system. The effects on differentiation in vivo were not evaluated, however, as the lesions resulting from implantation of CIC- or DNETV5 expressing BT88 cells were too small to provide meaningful cell numbers for assessment.

Taken together, however, our cumulative data from this work indicate that Cic regulates NSC proliferation and cell fate in neurodevelopment and oligodendroglioma, and that the pro-proliferative and pro-OPC phenotypes observed with Cic loss are largely mediated through de-repression of Ets factors.

DISCUSSION

Genomic analyses of brain cancers have suggested that *CIC* functions as a tumor suppressor gene in diffuse gliomas, particularly ODGs (3, 4, 37). Yet, to date, knowledge of *CIC*'s role in the brain has been limited. Here we report previously undescribed cell type specific differences in CIC expression in the brain. Moreover, our functional work examining *Cic* function in forebrain development and in oligodendroglioma cells provides new insight into the roles of this putative tumor suppressor in regulating the developmental fate of neural stem/progenitor cells.

We found that genetic ablation of Cic biases cells neural stem cells away from neuronal lineage specification to the selection of glial lineages. Adding to previous knowledge that RAS/MAPK pathway signaling regulates the switch from neurogenesis to gliogenesis, with *ETV5* implicated in mediating gliogenic competence (17, 35), our results firmly place *Cic* at the intersection of RAS pathway signaling and *Etv5* in the brain, providing a missing link between extrinsic differentiation signals and the execution of transcriptional programs critical for normal neuro- and glio-genesis. With respect to the Cic and the anti-neuronal bias that we observed, recent work by Lu, et al. found that disrupting Ataxin-1 (Atxn1)-Cic complexes resulted in abnormal maturation and maintenance of upper-layer cortical neurons – with concomitant effect on behavior, learning, and memory (14). It is unknown, however, the extent to which the effects could be due to specific Ataxin-Cic interactions versus Cic abnormality alone. Our studies, which primarily focused on early events, did not systematically address questions of neuronal maturation (although some of our in vitro findings are consistent with a neuronal maturation defect). Together, however, the cumulative data point to important roles for Cic in both initial specification as well as maintenance of neurons – highlighting the need for future work to define the complex neuronal dependencies on Cic, not only in the forebrain but also in the cerebellum where Cic pathology has also been implicated (38) (39).

With respect to neural stem cell proliferation, glial fates, and the implications for ODG; our findings build on the recent discovery that CIC deficiency increases proliferation and self-renewal of NSCs and results in an increased population of OPCs in the brain (13). In reporting these findings, our work also provides a foundation for understanding the relationship between *CIC* loss and ODG biology – as both dysregulated proliferation and the persistence of an immature OPC phenotype are cardinal features of this cancer. Many parallels exist between normal OPCs and the cells comprising ODG. In common, both OPCs and ODGs express PDGF, PDGFR, and NG2, which control OPC differentiation (40, 41). Together, the results may thus explain not only some of these phenotypic features of ODG, but are also consistent with other reports suggesting that dysregulation of OPCs or OPC-like cells are amongst the early changes in experimental models of gliomagenesis (2, 42).

There are some notable differences between the work reported by Yang, et al. (13), however, and our present studies. One difference is that the prior study used HOG cells that, despite their historic name, do not carry the ODG-defining genetic features of 1p19q loss or *CIC* mutation; similarly the Pdgfra-amplified/overexpressed mouse glioma model used is more akin to an RTK-driven GBM than it is to ODG. In deploying the BT-88 and BT-54 models (which genetically and phenotypically faithfully recapitulate ODG), our work may be closer to clinical relevance for ODG. Our studies also further clarify the early neuronal-glial fate decision effects of NSCs, with the bias away from neuronal fates and toward glial fates in the setting of CIC loss. Most importantly, however, we now identify *Etv5* de-repression as a key mechanism underlying much of the phenotypic effects in NSCs.

Our observation that *DN-Etv5* alone can abrogate so much of the pro-proliferative and pro-OPC phenotype resulting from *Cic* loss was somewhat unexpected. While it is possible that a single *Etv* gene is the primary effector, one caveat is that there is high similarity between Etv4 and Etv5, and our dominant negative construct may not be entirely specific for inhibiting Etv5 alone. Such cross-reactivity has been reported with similar approaches, and further experiments would be required to dissect the relative contribution of different Pea3/Ets factors. Although our Etv5 siRNA experiments lend some

independent support to the requirement for Etv5, it remains possible that there are collaborating or differential contributions of different Ets family members, particularly Etv4. Nevertheless, the identification of this family of genes as a likely mediator could be salient to the development of future therapeutic strategies for ODG. In addition to Etv5 constituting a major mechanism of action behind Cic loss-of-function effects, there are likely to be other important factors contributing to those responses as well – including the function of other potential direct targets of Cic transcriptional repression, and non-nuclear or non-transcriptional changes such as altered cellular metabolism (43).

Finally, although our findings are relevant to ODG biology, it is recognized that our studies do not directly model the genesis of ODG. Indeed, despite the increase in proliferation observed in Cic-null cells, no tumors were detected when following for up to one year after *Cre* electroporation of the *Cic* floxed mice (data not shown) – in keeping with the concept that several collaborating genetic hits are necessary for oncogenic transformation. Our *Cic* conditional knockout mice, however, will be a useful tool for a future more refined cell type- and stage-specific deletion of *Cic* along with the introduction of other mutations such as of *IDH1*(R132H) (44). We conceptualize *IDH1/2* mutations as a first event in ODG, causing epigenetic changes that that serve to expand the potential pool of cells vulnerable to transformation, with second-hit loss of *CIC* serving to dysregulate proliferation, bias cells to oligodendroglial lineage, and delay them in an immature state. Additional studies using experimental models and human ODG samples are needed to further dissect the relationship of *CIC* mutation to *IDH* mutation. Although one recent study used single-cell RNA-Seq to examine ODG cell subpopulations and did not detect any differences between ODG cells with and without *CIC* mutation, the number of cells analyzed was limiting for resolution, and functional studies were not performed (45). Similar approaches with larger cell numbers might provide further insight into the biology of ODG with respect to *CIC*.

In summary, we provide evidence that Cic regulates proliferation, fate decisions, and differentiation in neural stem cells, with loss particularly expanding the OPC population. Furthermore, our findings

indicate that disruption of the Cic-Etv axis (with abnormal de-repression of *Etv5* downstream of *Cic* loss) is central to the biology of ODG.

METHODS

Mice

CD1 outbred mice (Jackson Labs) were used for Cic expression analyses.

Cic conditional knockout (*Cic*-CKO) mice were generated at Taconic Artemis by homologous recombination to flank Cic exons 2-11 with loxP sites. The exons targeted are 2-11 of *Cic* short form, transcript variant 1, NM_027882.4 (equivalent to exons 3-12 of the *Cic* long form, NM_001302811.1, Cic transcript variant 4). The targeting vector was generated using clones from the C57BL/6J RPCIB-731 BAC library, and consisted of a 4.0 kb 5' flanking arm, neomycin resistance cassette (flanked by FRT sites), 5.5 kb loxP-flanked region, a puromycin resistance cassette (flanked by F3 sites), and 6.0 kb 3' flanking arm. After homologous recombination in C57BL/6N Tac ES cells, generation of chimeric animals, and germline transmission, Neo^R and $Puro^R$ cassettes were removed via Flp recombination by breeding with a Flp deleter line. The
final CIC-CKO allele carries loxP sites in introns 1 and 11, and single residual FRT and F3 sites. Expression of Cre recombinase results in deletion of exons 2-11 and frameshifting of the remaining CIC-S exons 12-20. Genotyping primers were as follows: CIC 5' flanking region (192 bp wt, 348 bp CKO allele) 5'- AGG AGG TTG TTA CTC GCT ATG G -3' (forward) and 5'- CTG ATG TCC TAA GAC CTT TAC AAG G -3' (reverse); CIC 3' flanking region (273 bp wt, 410 bp CKO) 5' – CTG TGT CAC TGT CTG CCT TCC -3' (forward) and 5' – TGG GTA ATA CCA CCG TGC C – 3 (reverse)'.

FoxG1-cre mice (Jackson Labs) were bred to *Cic*-CKO mice to generate telencephalic CIC knockouts and littermate controls. After euthanasia, dissected brains were processed for histology, western blotting, or cell culture. Knockout in tissue or cells post-cre was confirmed by Q-RT-PCR using primer/probe sets for CIC (Applied Biosystems) and by Western blotting with anti-Cic.

In all mouse experiments, the morning of vaginal plug was designated embryonic day 0.5 (E0.5). Both males and females were used.

In utero electroporation

In utero electroporation was performed as described previously [1] using the following plasmids: pLKO.1-Cic shRNA (Sigma, TRCN0000304642; 5'-CCG GAG CGG GAG AAG GAC CAT ATT CCT CGA GGA ATA TGG TCC TTC TCC CGC TTT TTT G-3'), pLKO.1-non-targeting shRNA (Sigma; 5'-CCT AAG GTT AAG TCG CCC TCG CTC GAG CGA GGG CGA CTT AAC CTT AGG -3'), pCIG2-Cre (which contains Cre-IRES-GFP), pCIC-ETV5 (which contains Etv5-IRES-mCherry), Super piggyBac Transposase (Systems Biosciences, SBI), and piggyBac cargo vector PB513B-1 (SBI) into which cDNAs were cloned for Turbo-Cre and Etv5. The DN-ETV5 consists of an *Etv5-EnR* fusion (gift of Dr. Carol Schuurmans) cloned into the piggyBac construct modified to contain the CAG promoter and GFP-luciferase. DNA was prepared with Endo-free DNA kit (Qiagen) and was injected at 1.5 µg/µl into the telencephalic vesicles of embryos in time-staged pregnant females using a Femtojet 4i microinjector (Eppendorf) then followed by electrical pulses (6 x 43 V, 950 ms interval) applied by platinum tweezer-style electrodes (7 mm, Protech) using a BTX square wave generator (Harvard Apparatus). Post-procedure, embryos were allowed to develop until the time of harvesting. EdU (50 mg/ml in PBS) was injected intraperitoneally into the pregnant dam 30 minutes prior to euthanasia.

Neural stem cell culture

The VZ of E15 brains were dissected, and tissue was dissociated to single cells using Accumax (EMD Millipore). Cells were grown at 37°C, 5% CO_2 in low-adhesion tissue culture flasks (Sarstedt) in mouse neural stem cell (mNSC) media consisting of NeuroCult Proliferation media (Stem Cell Technologies) supplemented with heparin, epidermal growth factor (EGF 20 ng/mL; Peprotech), and fibroblast growth factor (FGF 20 ng/mL; Peprotech). When spheres reached 100–200 µm in diameter, cells were split using Accumax and re-plated at 20,000 cells/mL.

Transfection of cultured cells

1-4 x 10^6 dissociated cells were re-suspended in 100 µL of Amaxa Mouse NSC Nucleofector Solution (VPG-1004, Lonza) with 5 µg of plasmid DNA. Nucleofection was performed with a Nucleofector II Device (Amaxa) using the A-033 program. Cells were returned to mouse neural stem cell media for further expansion/selection. For siRNA-mediated Etv5 knockdown, cells were transfected with 50 nM Etv5 ON-TARGET Plus SMARTpool siRNAs (Dharmacon) using Lipofectamine 3000 reagent per manufacturer's protocol. Cells were assayed 48hrs hours post-transfection.

Trypan Assay

150,000 cells were seeded per T25 flask in mNSC media and counted after 72 hours on a TC20 cell counter (Biorad) using Trypan blue stain (Thermo). Both dead and live cells were counted.

Neural Colony-Forming Cell Assay

Cells in semi-solid media were prepared using the Neurocult NCFC Assay Kit (Stem Cell Technologies) per manufacturer's protocol. Cells were plated at a density of 1,650 cells/ml using 1.5 ml per 35 mm culture dish. Dishes were replenished after 7 days with 60 µl of neural stem cell proliferation media supplemented with heparin, EGF, and FGF. Sphere number and size were scored using a gridded scoring dish (Stem Cell Technologies). 8-cell aggregates were used as the cut-off for scoring.

Lineage-directed differentiation

<u>Neuronal Differentiation:</u> NSCs were seeded in mNSC proliferation media (Stem Cell Technologies) on coverslips coated with Poly-L-Ornitihine and Laminin. After 24 hrs, media was replaced with Neurobasal Media, 2% B-27, 2mM GlutaMAX-I (Thermo). After 4 more days dibutyryl cAMP (Sigma) was added daily to a final concentration of 0.5 mM.

<u>Oligodendroglial Differentiation</u>: NSCs were seeded on coverslips coated with Poly-L-Ornitihine and Laminin. After 24 hrs, media was replaced with Neurobasal media, 2% B-27, GlutaMAX-I, 30 ng/mL 3,3',5-Triiodo-L-thyronine sodium (Sigma).

Astrocyte Differentiation: NSCs were seeded on coverslips coated with Geltrex (Thermo). After 24 hrs, media was replaced with DMEM, 1% N2-Supplement, 2mM GlutaMAX™-I, 1% FBS.

Immunostaining

Tissue was fixed overnight in 4% PFA, cryoprotected in 30% sucrose/PBS, and embedded in Tissue-Tek O.C.T. (Sakura Finetek) prior to cutting 6 µm cryosections on Superfrost Plus slides (VWR). Cultured cells grown on coverslips were fixed for 20 minutes in 4% PFA then rinsed in PBS. Permeabilization was performed with 1× TBST (Tris-buffered saline: 25 mM Tris, 0.14 M NaCl, 0.1% Triton X-100) for 15 min at room temperature (RT). 3% goat or horse serum in TBST x 30 min was used for block. Primary antibodies applied for 1 hr at RT or O/N at 4°C in block. Alexa Fluor secondary antibodies were applied at 1:500 dilution for 1 hour RT. Nuclei were counterstained in 4′,6-diamidino-2-phenylindole (DAPI; Santa Cruz) and mounted with FluorSave Reagent (Calbiochem). For immunostaining of tissue sections when two or more primary antibodies were from the same host species and for comparison of cell-type specific CIC expression, the Opal 4-colour IHC kit (PerkinElmer) was used per manufacturer's protocol.

Western blotting

Cells/tissue was lysed in RIPA buffer (10 mM Tris-Cl pH 8, 1 mM EDTA, 1% Triton X-100, 0.1% sodium deoxycholate, 0.1% SDS, 140 mM NaCl, 1 mM PMSF) with 1X Halt Protease and Phosphatase Inhibitor Cocktail (Thermo). 20 µg protein lysate (50 µg in the case of CIC probing) was run on 4-12% Bis-Tris or 3-8% Tris-Acetate gels (Thermo). Protein was transferred to PVDF membranes in NuPAGE Transfer Buffer (Thermo). Membranes were blocked in TBST with 5% powdered milk. Primary antibodies diluted were applied for 1 hr at room temperature or overnight at 4°C. Horseradish peroxidase-coupled secondary antibodies were applied for 1 hr at room temperature. Membranes were developed using ECL Plus Western Blotting Reagent (GE Healthcare) and X-ray film.

Transcriptional analysis

Total RNA was extracted using AllPrep DNA/RNA/Protein Mini Kit (Qiagen) per manufacturer's protocol. For each of 3 biologic replicates per condition, 100 ng RNA was subjected to nanoString analysis on nCounter system (NanoString Technologies) using a custom gene expression codeset containing neurodevelopmental and brain cancer associated genes, and 3 housekeeping genes. Data were analyzed using nSolver software and exported to PRISM software for further statistical analyses. Counts for Etv1, Etv4, and Etv5 were normalized to the average of 3 house-keeping genes (GAPDH, Actin, Tubulin beta chain).

In situ hybridization

Digoxygenin (DIG)-labeled riboprobes were prepared using a 10x DIG-labeling kit (Roche), and ISH was performed as described previously using probes for *GFP* and *Etv5* (17).

Chromatin immunoprecipitation

50 mg P6 mouse forebrain tissue was use per ChIP assay. ChIP was performed with the SimpleChip Plus Kit with magnetic beads (Cell Signaling) per manufacturer's protocol with the following exceptions. Tissue was disaggregated using a Dounce homogenizer. In place of micrococcal nuclease, shearing was performed on a UCD Bioruptor on high power with intervals of 30 seconds on, 1 minute off for 30 minutes. 1.5 µl of anti-CIC (PA1-46018, Thermo) was used per IP reaction. Histone H3 antibody and normal rabbit IgG were used as positive and negative controls, as supplied in the kit. PCR primers for the ETV5 promoter region were: 5′-GGTGCAGGCCGAGGCCAGGG-3′ (For) and 5′-CATTGACCAATCAGCACCGG-3′ (Rev).

Image Analysis

Coronal sections at the level of the anterior commissure were used in all quantitations of cell populations and staining intensities in the dorsal cerebral cortex and corpus callosum. Slides were imaged on AxioObserver fluorescence microscope (Zeiss). Images were processed using CS6 Photoshop software (Adobe) for orientation, false colorization, and overlay/colocalization. Enumeration of cells positive for

cytoskeletal, cytoplasmic or membrane proteins was performed manually by counting positive cells using the Photoshop CS6 counting tool. Quantitation of CIC nuclear staining intensity and MBP staining density was performed using FIJI software (46) as follows. Images were first processed using Gaussian blur, then background subtracted. Default threshold limits were used in the threshold tool. Images were converted to binary and watershed was run to separate clumped cells. Nuclear staining was quantitated by using the analysing particles option with separate cut-offs set for each antibody used. For quantitation of MBP expression on tissue sections, FIJI was used by drawing regions of interest on the lateral corpus callosum (cingulum), and the mean integrated density in the regions of interest was calculated.

Intracranial BTIC xenografts and Bioluminescence imaging

1×10^5 BT88 cells stably transfected with CIC-GFP-Luciferase or DNETV5-GFP or respective empty vectors were stereotactically implanted into the right striata of 6- to 8-week-old NOD/SCID mice. 6 weeks post-implantation, tumour burden was measured either by bioluminescence imaging using IVIS Spectrum In Vivo Imaging System (Xenogen) and/or by histology from euthanized animals. Mice were anaesthetized under isoflurane and intraperitoneal injection of XenoLight D-Luciferin (PerkinElmer) was administered at a dose of 150mg/kg body weight. Acquisition of bioluminescence images was performed 10 min post-injection. Analysis was performed using Living Image Software by measurement of photon counts (photon/s/cm^2) with a region of interest drawn around the bioluminescence signal.

Statistics

Data are represented as mean ± SD from at least 3 biologic replicates for experiments. Comparisons between experimental and control samples were made using 2-tailed t-test or, when there were more than 2 group, using ANOVA. Tukey's procedure was applied post-hoc to correct for multiple comparisons during multiple pairwise analyses (e.g. differential Cic expression among cell types).

Bonferroni post-hoc correction was applied for statistical analysis of data from NanoString assays. Statistical analyses were performed using Prism sofware (Graphpad).

Study Approval

Animal use was approved by the University of Calgary Animal Care Committee (protocol AC16-0266) in compliance with the Guidelines of the Canadian Council of Animal Care.

AUTHOR CONTRIBUTIONS

Conceptualization, JAC, STA; Methodology, JAC, CS, STA; Investigation, STA, ADR, RD, LF, MJC, MA, WW, SOL; Acquisition, Analyses and Interpretation of data, JAC, STA; Writing – Original Draft, JAC, STA; Writing – Review & Editing, JAC, SC, JGC, SMR, MAM, WW, RD, SOL; Funding Acquisition, JAC, JGC, CS; Resources, LA, MA, CS; Supervision, JAC, CS, JGC, SMR.

ACKNOWLEDGEMENTS

This work was funded by Canadian Institutes for Health Research (JAC), Cancer Research Society (CS, JAC), Alberta Cancer Foundation (STA, ADR, LF, JGC), Alberta Innovates Health Solutions (JAC, CS).

COMPETING FINANCIAL INTERESTS

The authors have no competing financial interests to declare.

REFERENCES

1. Reifenberger G, Kros JM, Louis DN, and Collins VP. In: Louis DN, Ohgaki H, Wiestler OD, and Cavenee WK eds. *WHO Classification of Tumours of the Central Nervous System*. Lyon: International Agency for Research on Cancer (IARC); 2016:54-62.
2. Persson AI, Petritsch C, Swartling FJ, Itsara M, Sim FJ, Auvergne R, et al. Non-stem cell origin for oligodendroglioma. *Cancer Cell.* 2010;18(6):669-82.
3. Yip S, Butterfield YS, Morozova O, Chittaranjan S, Blough MD, An J, et al. Concurrent CIC mutations, IDH mutations, and 1p/19q loss distinguish oligodendrogliomas from other cancers. *J Pathol.* 2012;226(1):7-16.
4. Bettegowda C, Agrawal N, Jiao Y, Sausen M, Wood LD, Hruban RH, et al. Mutations in CIC and FUBP1 contribute to human oligodendroglioma. *Science.* 2011;333(6048):1453-5.
5. Cancer Genome Atlas Research N, Brat DJ, Verhaak RG, Aldape KD, Yung WK, Salama SR, et al. Comprehensive, Integrative Genomic Analysis of Diffuse Lower-Grade Gliomas. *N Engl J Med.* 2015;372(26):2481-98.
6. Jimenez G, Shvartsman SY, and Paroush Z. The Capicua repressor - a general sensor of RTK signaling in development and disease. *Journal of cell science.* 2012;125(Pt 6):1383-91.
7. Lohr U, Chung HR, Beller M, and Jackle H. Antagonistic action of Bicoid and the repressor Capicua determines the spatial limits of Drosophila head gene expression domains. *Proc Natl Acad Sci U S A.* 2009;106(51):21695-700.
8. Ajuria L, Nieva C, Winkler C, Kuo D, Samper N, Andreu MJ, et al. Capicua DNA-binding sites are general response elements for RTK signaling in Drosophila. *Development.* 2011;138(5):915-24.
9. Grimm O, Zini VS, Kim Y, Casanova J, Shvartsman SY, and Wieschaus E. Torso RTK controls Capicua degradation by changing its subcellular localization. *Development.* 2012;139(21):3962-8.

10. Astigarraga S, Grossman R, Diaz-Delfin J, Caelles C, Paroush Z, and Jimenez G. A MAPK docking site is critical for downregulation of Capicua by Torso and EGFR RTK signaling. *The EMBO journal.* 2007;26(3):668-77.

11. Lim B, Samper N, Lu H, Rushlow C, Jimenez G, and Shvartsman SY. Kinetics of gene derepression by ERK signaling. *Proc Natl Acad Sci U S A.* 2013;110(25):10330-5.

12. Dissanayake K, Toth R, Blakey J, Olsson O, Campbell DG, Prescott AR, et al. ERK/p90(RSK)/14-3-3 signalling has an impact on expression of PEA3 Ets transcription factors via the transcriptional repressor capicua. *The Biochemical journal.* 2011;433(3):515-25.

13. Yang R, Chen LH, Hansen LJ, Carpenter AB, Moure CJ, Liu H, et al. Cic Loss Promotes Gliomagenesis via Aberrant Neural Stem Cell Proliferation and Differentiation. *Cancer Res.* 2017;77(22):6097-108.

14. Lu HC, Tan Q, Rousseaux MW, Wang W, Kim JY, Richman R, et al. Disruption of the ATXN1-CIC complex causes a spectrum of neurobehavioral phenotypes in mice and humans. *Nat Genet.* 2017;49(4):527-36.

15. Graham V, Khudyakov J, Ellis P, and Pevny L. SOX2 functions to maintain neural progenitor identity. *Neuron.* 2003;39(5):749-65.

16. Faedo A, Borello U, and Rubenstein JL. Repression of Fgf signaling by sprouty1-2 regulates cortical patterning in two distinct regions and times. *J Neurosci.* 2010;30(11):4015-23.

17. Li S, Mattar P, Dixit R, Lawn SO, Wilkinson G, Kinch C, et al. RAS/ERK signaling controls proneural genetic programs in cortical development and gliomagenesis. *J Neurosci.* 2014;34(6):2169-90.

18. Kriegstein A, and Alvarez-Buylla A. The glial nature of embryonic and adult neural stem cells. *Annual review of neuroscience.* 2009;32:149-84.

19. Lim DA, and Alvarez-Buylla A. The Adult Ventricular-Subventricular Zone (V-SVZ) and Olfactory Bulb (OB) Neurogenesis. *Cold Spring Harb Perspect Biol.* 2016;8(5).

20. Lu QR, Sun T, Zhu Z, Ma N, Garcia M, Stiles CD, et al. Common developmental requirement for Olig function indicates a motor neuron/oligodendrocyte connection. *Cell.* 2002;109(1):75-86.

21. Zhou Q, Choi G, and Anderson DJ. The bHLH transcription factor Olig2 promotes oligodendrocyte differentiation in collaboration with Nkx2.2. *Neuron.* 2001;31(5):791-807.

22. Fores M, Simon-Carrasco L, Ajuria L, Samper N, Gonzalez-Crespo S, Drosten M, et al. A new mode of DNA binding distinguishes Capicua from other HMG-box factors and explains its mutation patterns in cancer. *PLoS Genet.* 2017;13(3):e1006622.

23. Jimenez G, Guichet A, Ephrussi A, and Casanova J. Relief of gene repression by torso RTK signaling: role of capicua in Drosophila terminal and dorsoventral patterning. *Genes Dev.* 2000;14(2):224-31.

24. Lee CJ, Chan WI, Cheung M, Cheng YC, Appleby VJ, Orme AT, et al. CIC, a member of a novel subfamily of the HMG-box superfamily, is transiently expressed in developing granule neurons. *Brain research Molecular brain research.* 2002;106(1-2):151-6.

25. Kawamura-Saito M, Yamazaki Y, Kaneko K, Kawaguchi N, Kanda H, Mukai H, et al. Fusion between CIC and DUX4 up-regulates PEA3 family genes in Ewing-like sarcomas with t(4;19)(q35;q13) translocation. *Hum Mol Genet.* 2006;15(13):2125-37.

26. Hebert JM, and McConnell SK. Targeting of cre to the Foxg1 (BF-1) locus mediates loxP recombination in the telencephalon and other developing head structures. *Dev Biol.* 2000;222(2):296-306.

27. Kang P, Lee HK, Glasgow SM, Finley M, Donti T, Gaber ZB, et al. Sox9 and NFIA coordinate a transcriptional regulatory cascade during the initiation of gliogenesis. *Neuron.* 2012;74(1):79-94.

28. Stolt CC, Lommes P, Sock E, Chaboissier MC, Schedl A, and Wegner M. The Sox9 transcription factor determines glial fate choice in the developing spinal cord. *Genes Dev.* 2003;17(13):1677-89.

29. Bergles DE, and Richardson WD. Oligodendrocyte Development and Plasticity. *Cold Spring Harb Perspect Biol.* 2015;8(2):a020453.

30. Kuhlbrodt K, Herbarth B, Sock E, Hermans-Borgmeyer I, and Wegner M. Sox10, a novel transcriptional modulator in glial cells. *J Neurosci.* 1998;18(1):237-50.

31. Stolt CC, Rehberg S, Ader M, Lommes P, Riethmacher D, Schachner M, et al. Terminal differentiation of myelin-forming oligodendrocytes depends on the transcription factor Sox10. *Genes Dev.* 2002;16(2):165-70.

32. Lee Y, Fryer JD, Kang H, Crespo-Barreto J, Bowman AB, Gao Y, et al. ATXN1 protein family and CIC regulate extracellular matrix remodeling and lung alveolarization. *Dev Cell.* 2011;21(4):746-57.

33. Padul V, Epari S, Moiyadi A, Shetty P, and Shirsat NV. ETV/Pea3 family transcription factor-encoding genes are overexpressed in CIC-mutant oligodendrogliomas. *Genes Chromosomes Cancer.* 2015;54(12):725-33.

34. Crespo-Barreto J, Fryer JD, Shaw CA, Orr HT, and Zoghbi HY. Partial loss of ataxin-1 function contributes to transcriptional dysregulation in spinocerebellar ataxia type 1 pathogenesis. *PLoS Genet.* 2010;6(7):e1001021.

35. Li X, Newbern JM, Wu Y, Morgan-Smith M, Zhong J, Charron J, et al. MEK Is a Key Regulator of Gliogenesis in the Developing Brain. *Neuron.* 2012;75(6):1035-50.

36. Kelly JJ, Blough MD, Stechishin OD, Chan JA, Beauchamp D, Perizzolo M, et al. Oligodendroglioma cell lines containing t(1;19)(q10;p10). *Neuro Oncol.* 2010;12(7):745-55.

37. Davoli T, Xu AW, Mengwasser KE, Sack LM, Yoon JC, Park PJ, et al. Cumulative haploinsufficiency and triplosensitivity drive aneuploidy patterns and shape the cancer genome. *Cell.* 2013;155(4):948-62.

38. Lam YC, Bowman AB, Jafar-Nejad P, Lim J, Richman R, Fryer JD, et al. ATAXIN-1 interacts with the repressor Capicua in its native complex to cause SCA1 neuropathology. *Cell.* 2006;127(7):1335-47.

39. Rousseaux MWC, Tschumperlin T, Lu HC, Lackey EP, Bondar VV, Wan YW, et al. ATXN1-CIC Complex Is the Primary Driver of Cerebellar Pathology in Spinocerebellar Ataxia Type 1 through a Gain-of-Function Mechanism. *Neuron.* 2018;97(6):1235-43 e5.

40. Cairncross G, and Jenkins R. Gliomas with 1p/19q codeletion: a.k.a. oligodendroglioma. *Cancer journal.* 2008;14(6):352-7.

41. Shoshan Y, Nishiyama A, Chang A, Mork S, Barnett GH, Cowell JK, et al. Expression of oligodendrocyte progenitor cell antigens by gliomas: implications for the histogenesis of brain tumors. *Proc Natl Acad Sci U S A.* 1999;96(18):10361-6.

42. Liu C, Sage JC, Miller MR, Verhaak RG, Hippenmeyer S, Vogel H, et al. Mosaic analysis with double markers reveals tumor cell of origin in glioma. *Cell.* 2011;146(2):209-21.

43. Chittaranjan S, Chan S, Yang C, Yang KC, Chen V, Moradian A, et al. Mutations in CIC and IDH1 cooperatively regulate 2-hydroxyglutarate levels and cell clonogenicity. *Oncotarget.* 2014;5(17):7960-79.

44. Pirozzi CJ, Carpenter AB, Waitkus MS, Wang CY, Zhu H, Hansen LJ, et al. Mutant IDH1 Disrupts the Mouse Subventricular Zone and Alters Brain Tumor Progression. *Mol Cancer Res.* 2017.

45. Tirosh I, Venteicher AS, Hebert C, Escalante LE, Patel AP, Yizhak K, et al. Single-cell RNA-seq supports a developmental hierarchy in human oligodendroglioma. *Nature.* 2016;539(7628):309-13.

46. Schindelin J, Arganda-Carreras I, Frise E, Kaynig V, Longair M, Pietzsch T, et al. Fiji: an open-source platform for biological-image analysis. *Nat Methods.* 2012;9(7):676-82.

FIGURES

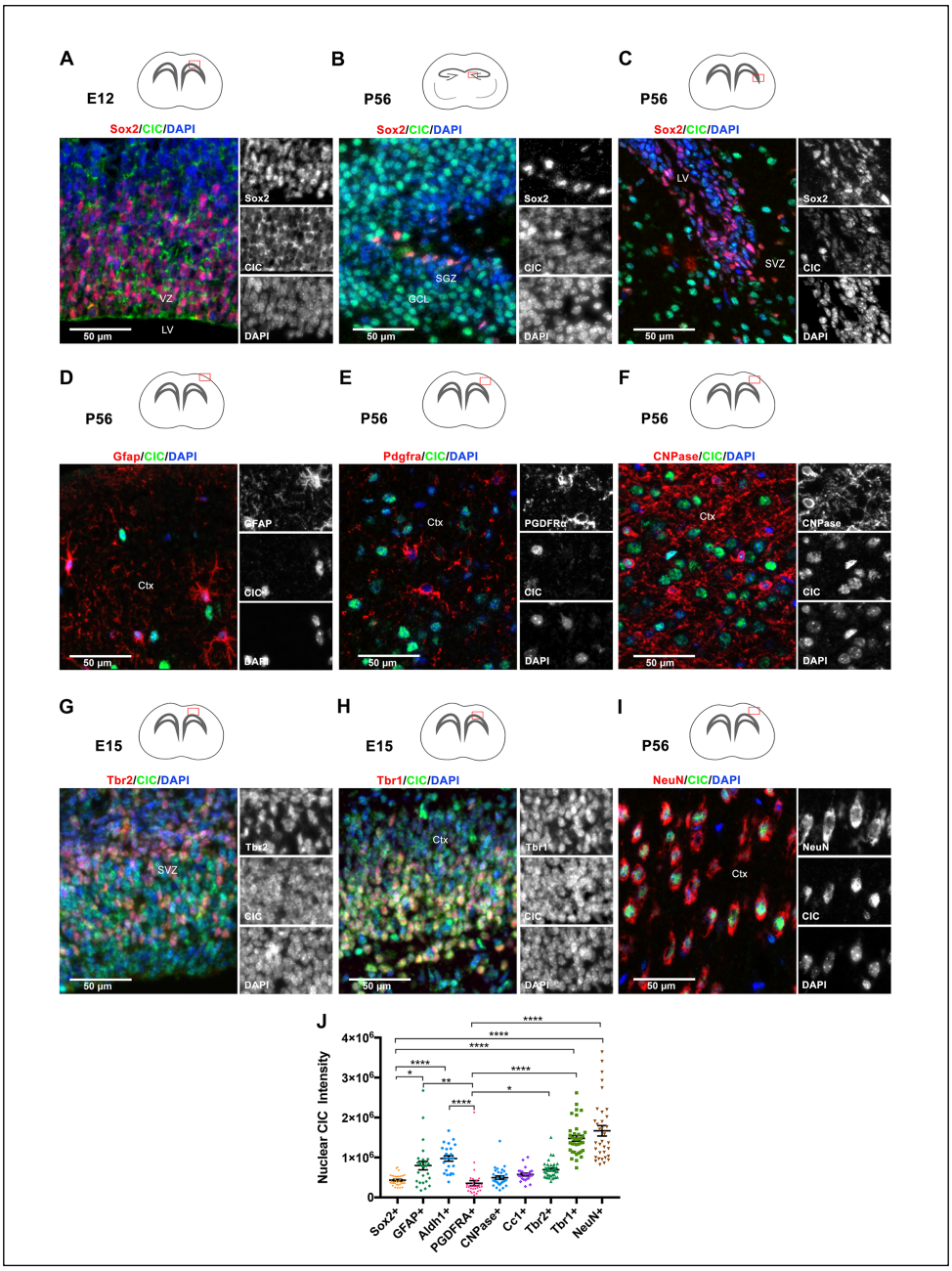

FIGURE 1: Differential Cic expression among cell types in the developing and mature brain. Representative images of immunofluorescence staining for Cic expression in Sox2+ stem cell populations in (A) E12 subventricular zone, (B) P56 hippocampal dentate gyrus subgranular zone, and (C) P56 subventricular zone. Cic expression in glial cells in the adult brain showing localization in (D) Gfap+ cortical astrocytes, (E) Pdgfra+ white matter OPCs, and (F) CNPase+ mature oligodendrocytes. Cic expression in cortical neuronal populations (G) E15 Tbr2+ early-born neurons in the SVZ and IZ, (H) E15 Tbr1+ late-born neurons in the cortical plate, and (I) adult post-mitotic NeuN+ cortical neurons. (J) Quantitation of Cic nuclear staining intensities, plotted for different brain cell types. Each point represents one cell quantitated. Results show quantitation from a minimum of 24 cells per marker from the boxed regions used for image analysis. Pairwise comparisons between cell types performed by ANOVA with

Tukey's posthoc test. Data shown as mean ± SD. *p<0.05, **p<0.01, ****p<0.0001. LV–lateral ventricle, GCL–granule cell layer, SGZ–subgranular zone, SVZ–subventricular zone, Ctx–cortex.

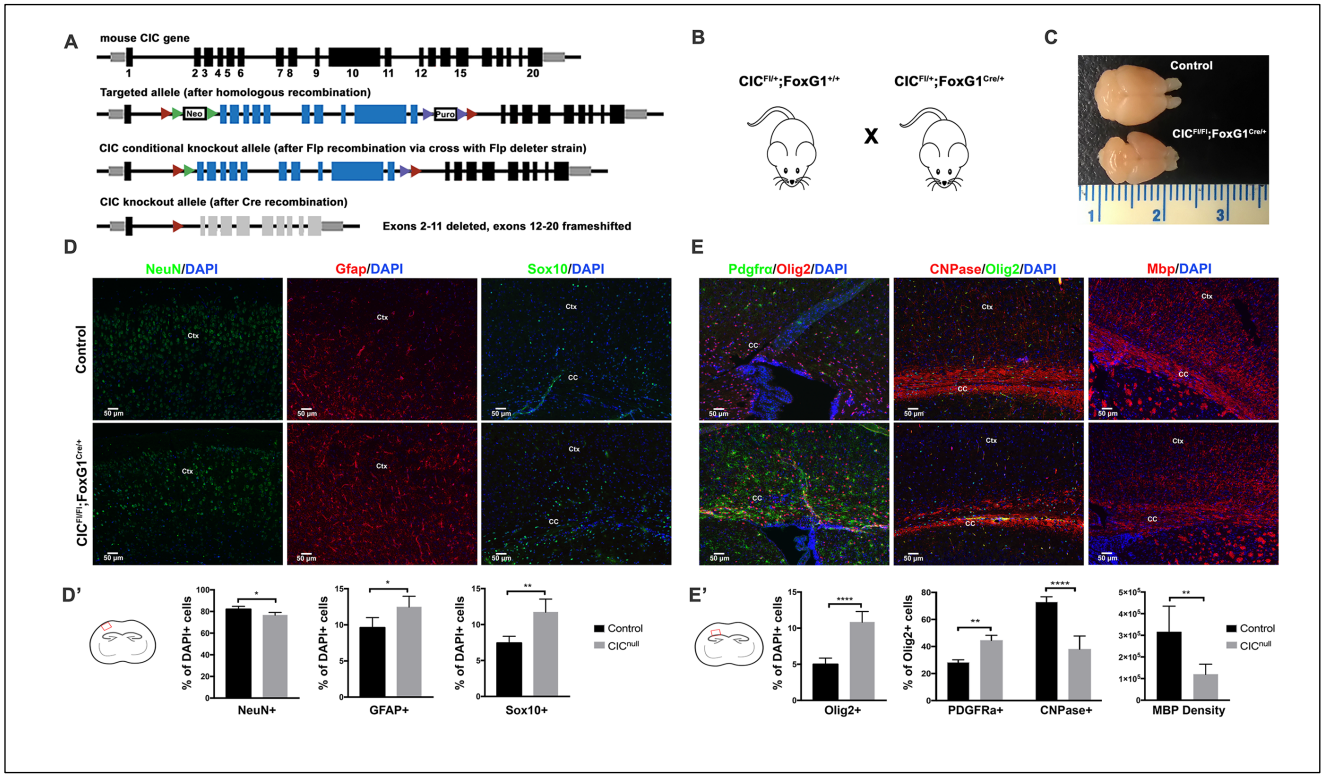

FIGURE 2: Forebrain-specific *Cic* deletion increases glial cells at the expense of neurons by P21 (A) Targeting strategy for Cic conditional knockout mice. Exon numbering is shown relative to Cic transcript variant 1. (B) Forebrain-deletion of Cic starting from E10.5 by crossing CIC-floxed line with FoxG1-cre. *Cic*$^{Fl/Fl}$*;FoxG1*$^{Cre/+}$ animals are compared with *Cic*$^{Fl/+}$*;FoxG*$^{Cre/+}$ or *Cic*$^{Fl/Fl}$*;FoxG1*$^{+/+}$ as controls. (C) Representative gross morphology of *Cic*-deleted and *Cic*-wildtype brains at P21. (D,D') Staining and quantitation of NeuN+, Gfap+, and Sox10+ cells in Cic-deleted (*Cic*$^{Fl/Fl}$*;FoxG1*$^{Cre/+}$) cortex vs control (*Cic*$^{Fl/Fl}$*;FoxG1*$^{+/+}$). (E,E') Staining and quantitation of Olig2+, Pdgfra+, and CNPase+ cells in lateral corpus callosum, and Mbp expression in lateral corpus callosum at P21. Results show quantitation from 5 mice per each group. Statistical analyses performed by unpaired t-test. Data shown as mean ± SD. *p<0.05, **p<0.01, ****p<0.0001. Ctx–cortex, CC–corpus callosum.

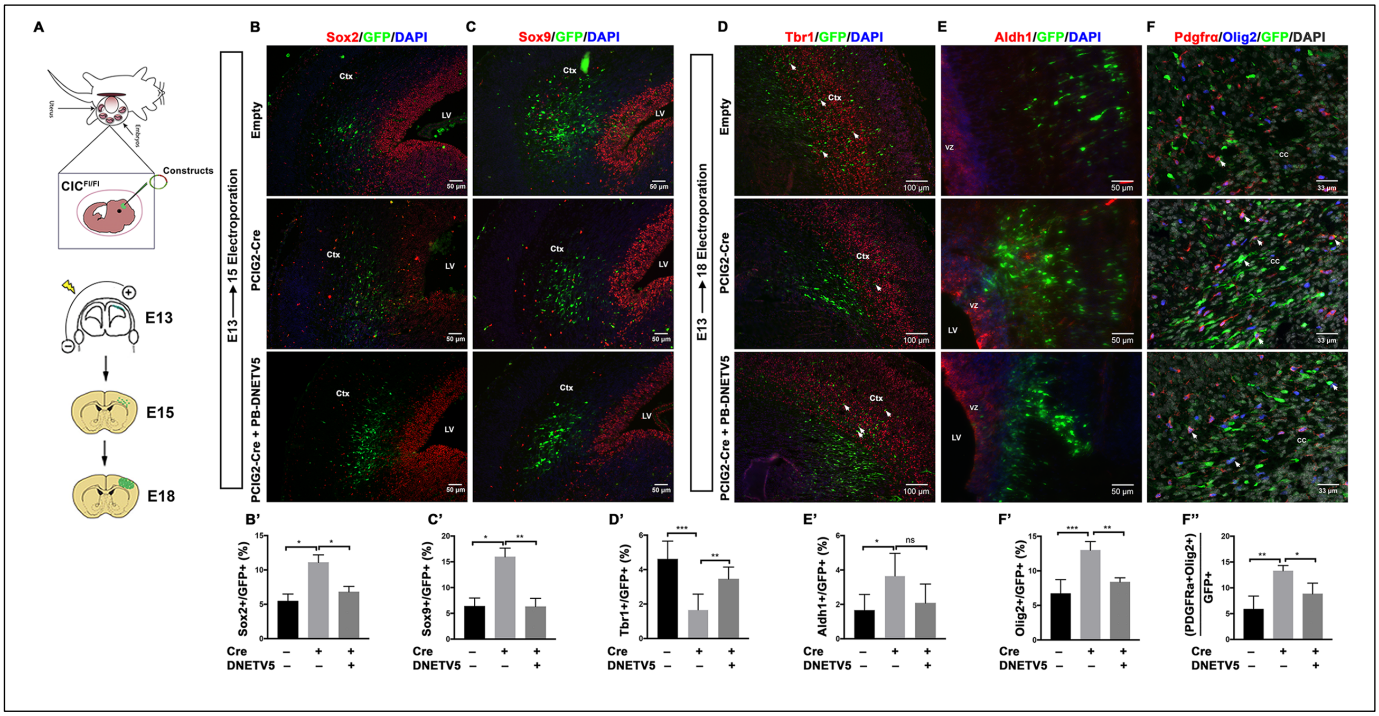

FIGURE 3: Deletion of *Cic* in the neurogenic period biases neural stem/progenitor cells to glial lineage selection. (A) Localized deletion of *Cic* in neural stem cells via *in-utero* electroporation into VZ cell of *C*ic-floxed embryos. Targeted cells carry a fluorescent marker and express either cre recombinase (Cre), dominant negative ETV5 (DNETV5), or not (Empty control), depending on the electroporated plasmid. Staining and quantitation of Sox2+ stem cells (B,B') and Sox9+ glioblasts (C,C') 2 days after E13 electroporation. Staining and quantitation of late-born Tbr1+ neurons, Aldh1+ astrocytes, Olig2+ oligodendrogial lineage cells, and Pdgfra+ oligodendrocyte precursors cells 5 days after E13 electroporation. Results show quantitation from 4 mice per group. Statistical analyses between control and experimental groups performed by ANOVA with Tukey's posthoc test. Data shown as mean ± SD. *p<0.05, **p<0.01, ***p<0.001, ns–not significant. Ctx–cortex, LV–lateral ventricle, VZ–ventricular zone.

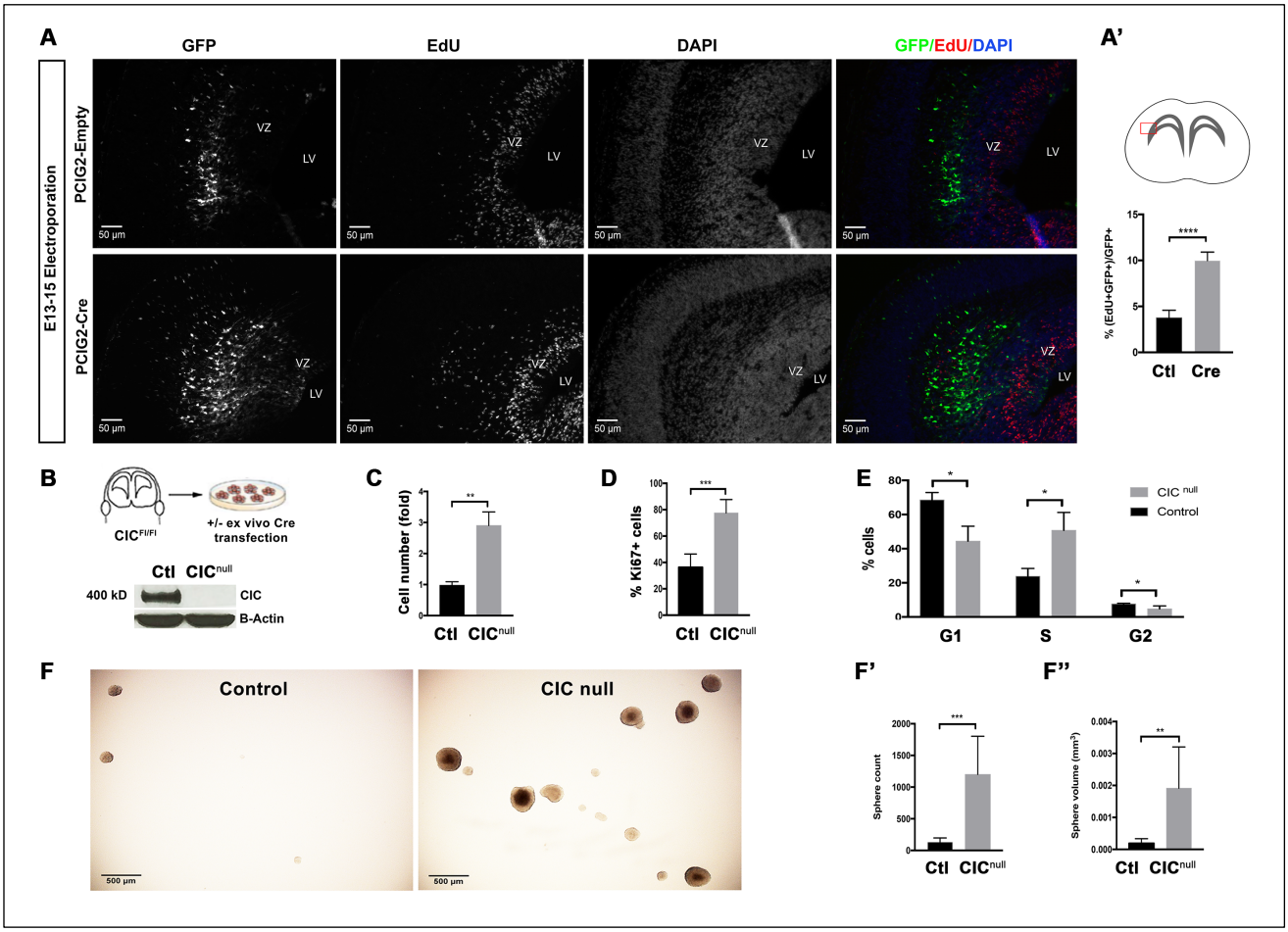

FIGURE 4: Cic deficiency increases proliferation and self-renewal of neural stem/progenitor cells. (A,A') EdU incorporation 48-hours after electroporation of *Cre* or control plasmid into VZ of E13 *Cic*-floxed embryos; boxed area indicates zone for imaging and quantitation (n ≥ 4 mice per group). (B) Generation of Cic-null cells and control cells from *Cic*-floxed cells via ex vivo transfection of Cre recombinase, and western blotting for validation of knockout. (C) Trypan blue assay, (D) Ki67 proliferation index, and (E) propidium iodide cell cycle analysis in cultured cells. (F) Neural colony forming assay with quantitation of (F') sphere number and (F'') sphere size. Data shown as mean ± SD. Data from ≥ 3 biologic replicates per condition. Statistical analysis performed by unpaired t-test. ns-not significant, *p<0.05, **p<0.01, ***p<0.001, ****p<0.0001. VZ–ventricular zone, LV–lateral ventricle.

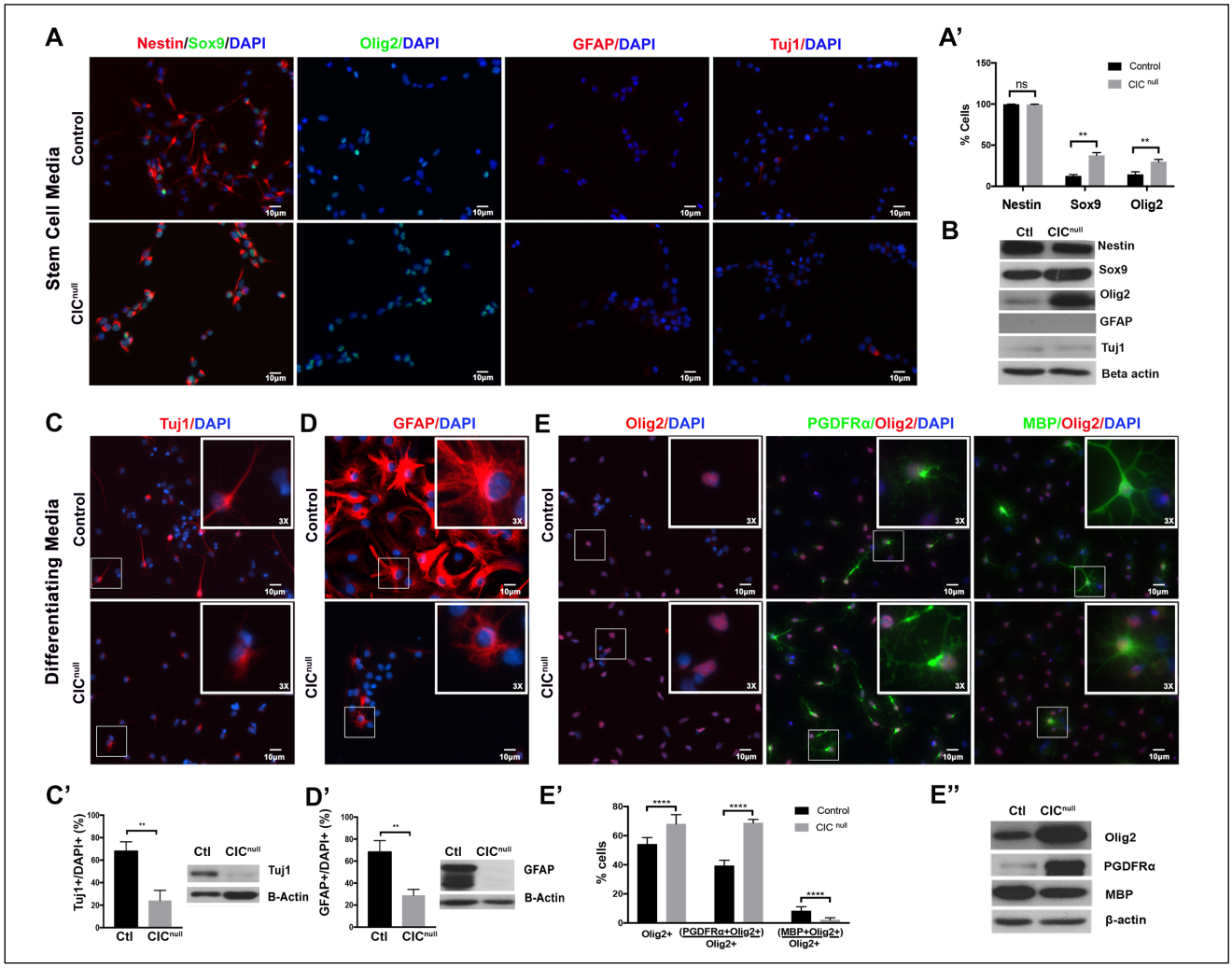

FIGURE 5: Cultured Cic null cells are oligodendrocyte lineage biased but stall in maturation at the OPC stage. (A) Immunofluorescence and (B) Western blotting for Nestin, Sox9, Olig2, Gfap, and Tuj1 in Cic-null and control cells cultured in stem cell conditions. Responses of Cic-null and control cells to 10-day exposure to lineage-directed differentiation conditions for (C) neurons, (D) astrocytes, or (E) oligodendrocytes. Immunofluorescence quantitation of cell populations and western blotting of cells cultured in lineage-directed differentiation conditions for (C') neurons, (D') astrocytes, and (E', E'') stages of oligodendrocyte development. Data shown as mean ± SD. Data from ≥ 3 biologic replicates per condition. Statistical analysis performed by unpaired t-test. ns-not significant, **p<0.01, ****p<0.0001.

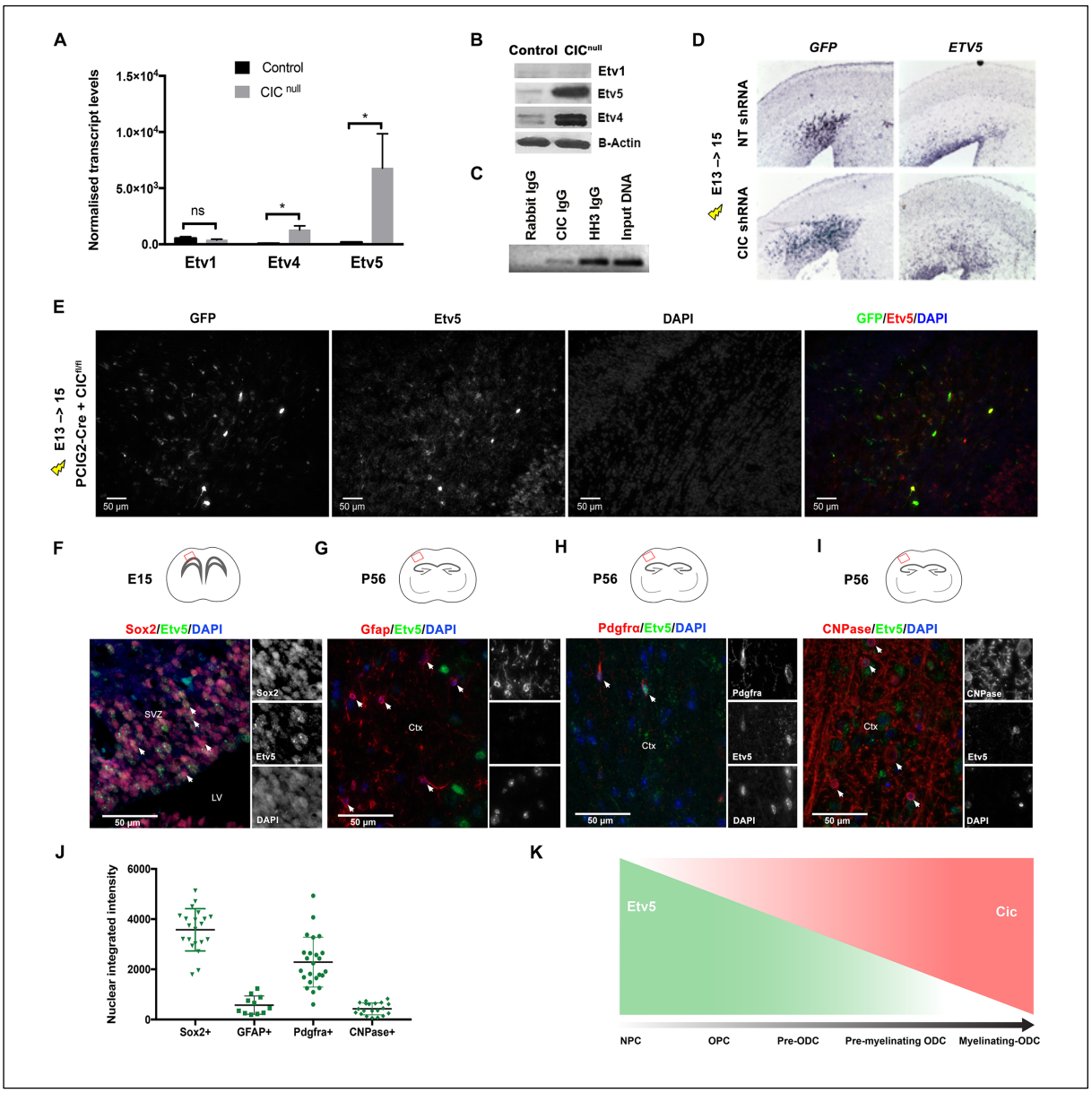

FIGURE 6: *Etv5* is a direct target of Cic transcriptional repression. *Etv1*, *Etv4*, and *Etv5* mRNA (A) and protein (B) levels in cultured CIC-null and -control cells after 48-hour exposure to oligodendrocytic differentiating conditions; transcript levels normalized to average of 3 (Actin, GAPDH, Tubulin beta chain) housekeeping genes. Data from n=3 biologic replicates. (C) ChIP-PCR for Cic at the *Etv5* promoter. (D) Electroporation of Cic shRNA or non-targeting (NT*)* shRNA at E13 followed by *in-situ* hybridization for *Etv5* and *GFP* at E15; *Etv5* transcripts are upregulated in areas of Cic knockdown. Data from n≥3 mice per group. (E) Immunofluorescence staining showing Etv5 and GFP protein expression 2 days after Cre electroporation into E13 VZ of *Cic*-floxed embryos. *Cic* deleted cells show increased Etv5 protein. (F-I, J) Differential Etv5 expression in (F) NSCs (Sox2+) at mid-neurogenesis, and in (G) astrocytes (Gfap+), (H) OPCs (Pdgfra+), and (I) mature oligodendrocytes (CNPase+) in P56 adult cortex. Each point represents one cell quantitated. Results show quantitation from ≥20 cells for each marker. Data shown as mean ± SD. Statistical analyses performed by unpaired t-test. *p<0.05. SVZ–subventricular zone, LV–lateral ventricle, Ctx–cortex. (K) Schematic depiction of relationship of Cic and Etv5 expression as neural stem cells differentiate to mature myelinating oligodendrocytes.

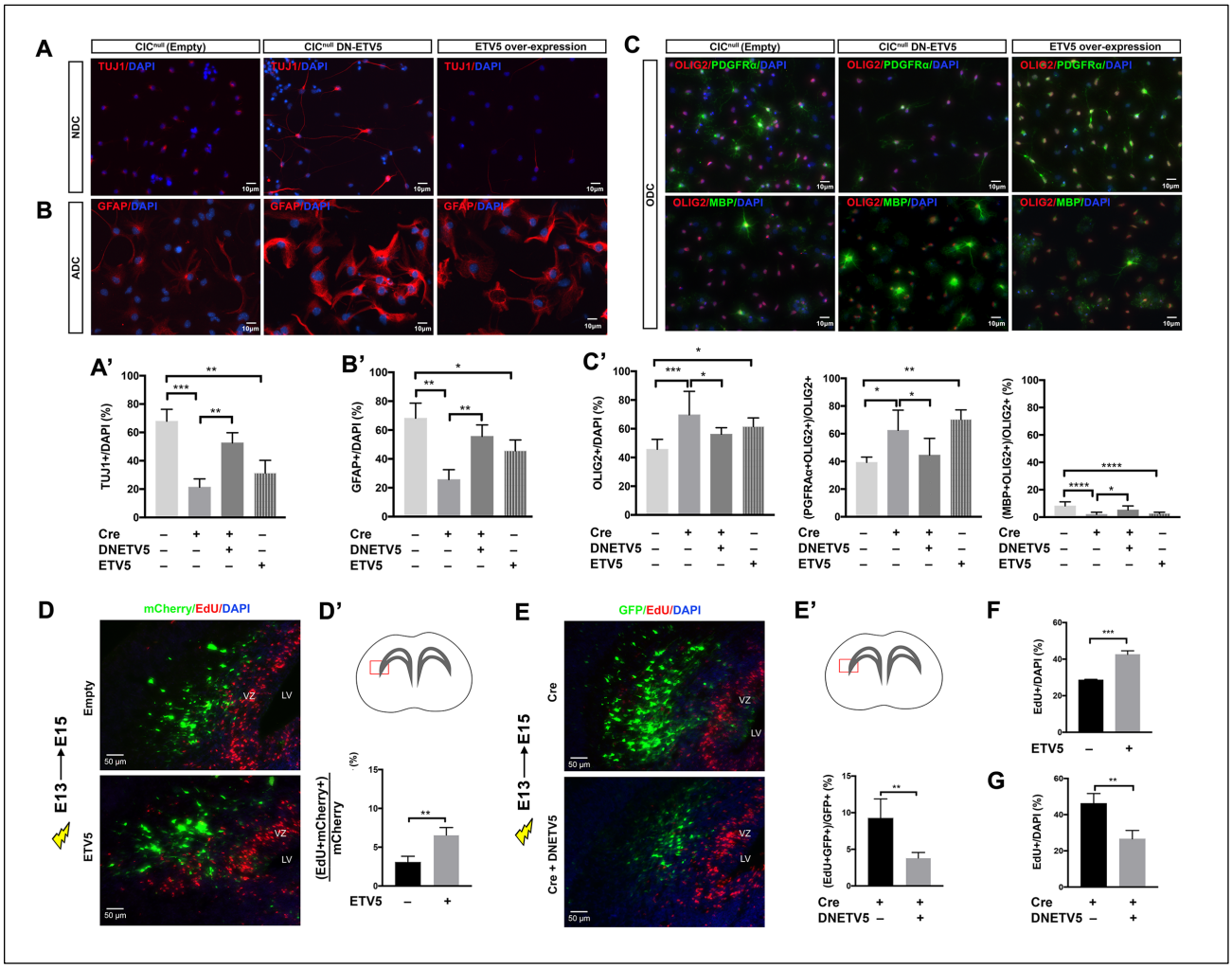

FIGURE 7: Etv5 is necessary and sufficient for proliferation and cell fate bias effects downstream of Cic loss. Cic-null cells with and without DN-ETV5, and Cic-wildtype cells with Etv5 overexpression were assessed for their ability to differentiate in response to 10-days' exposure to lineage-directed differentiating conditions. (A,A') Neuronal differentiation capacity was assessed by bIII-Tubulin immunostaining (Tuj1 positivity), (B,B') astrocytic differentiation capacity was assessed by Gfap immunostaining, and (C,C') oligodendroglial differentiation capacity was assess by staining for Olig2, Pdgfra, and Mbp. (D,D') EdU incorporation 2 days post-electroporation of wildtype *ETV5* or empty control plasmid, both carrying mCherry as a marker, into E13 CIC$^{Fl/Fl}$ VZ. Note: mCherry fluorescence and EdU staining were false-colorized to green and red after grayscale imaging. (E,E') EdU incorporation 2 days post-electroporation of Cre only or of Cre co-electroporated with *DN-ETV5* into E13 CIC$^{Fl/Fl}$ VZ . EdU incorporation assay in cultured NSCs showing (F) effects of ETV5 overexpression in CIC-wildtype NSCs and (G) effects of *DN-ETV5* expression in Cic-null NSCs. Data shown as mean ± SD from n ≥ 4 mice per each group for in vivo studies and n=3 biological replicates for cell culture studies. Statistical analyses performed either t-test in D', E', F, G; or with ANOVA with Tukey's posthoc test in A', B', C'. ns-not significant, *p<0.05, **p<0.01, ***p<0.0001. ADC–astrocytic differentiation condition, NDC–neuronal differentiation condition, ODC–oligodendrocytic differentiation condition. VZ–ventricular zone, LV–lateral ventricle.

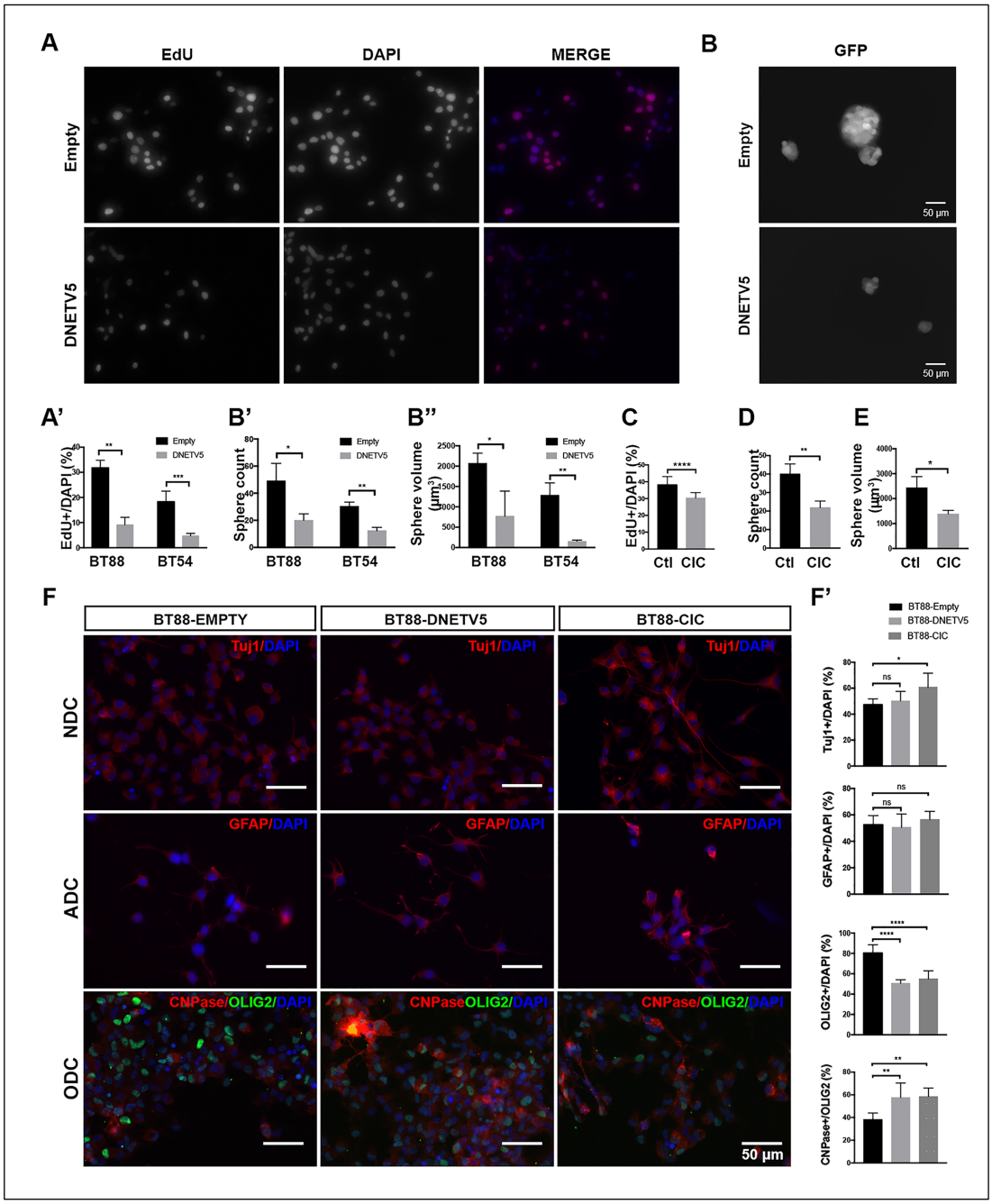

FIGURE 8: ODG cells require CIC loss or elevated ETV5 to maintain proliferation and stemness. (A,A') EdU incorporation in BT-88 and BT-54 ODG cell lines stably transfected with control plasmid or of DNETV5. Quantitation shows results from both cell lines. Representative images are from BT-88. (B) Representative images showing effect of DN-ETV5 on sphere formation in BT88 ODG cells. Quantification of (B') sphere number and (B") size in BT-54 and BT-88 ODG cells without and with DNETV5. (C,D,E) CIC re-expression in BT-88 cells decreases proliferation, sphere number, and sphere size. (F,F') Lineage-specific differentiation capacity of BT-88 ODG cells stably transfected with either control plasmid, DNETV5, or CIC; expression of Tuj1, GFAP, OLIG2, and CNPase after 10-days exposure to differentiation conditions for neurons, astrocytes, and oligodendrocytes. Data shown as mean ± SD from n=3 biologic replicates. Statistical analyses by ANOVA with Tukey's posthoc test. ns-not significant, *p<0.05, **p<0.01, ****p<0.0001. NDC–neuronal differentiation condition, ADC–astrocytic differentiation condition, ODC–oligodendrocytic differentiation condition.

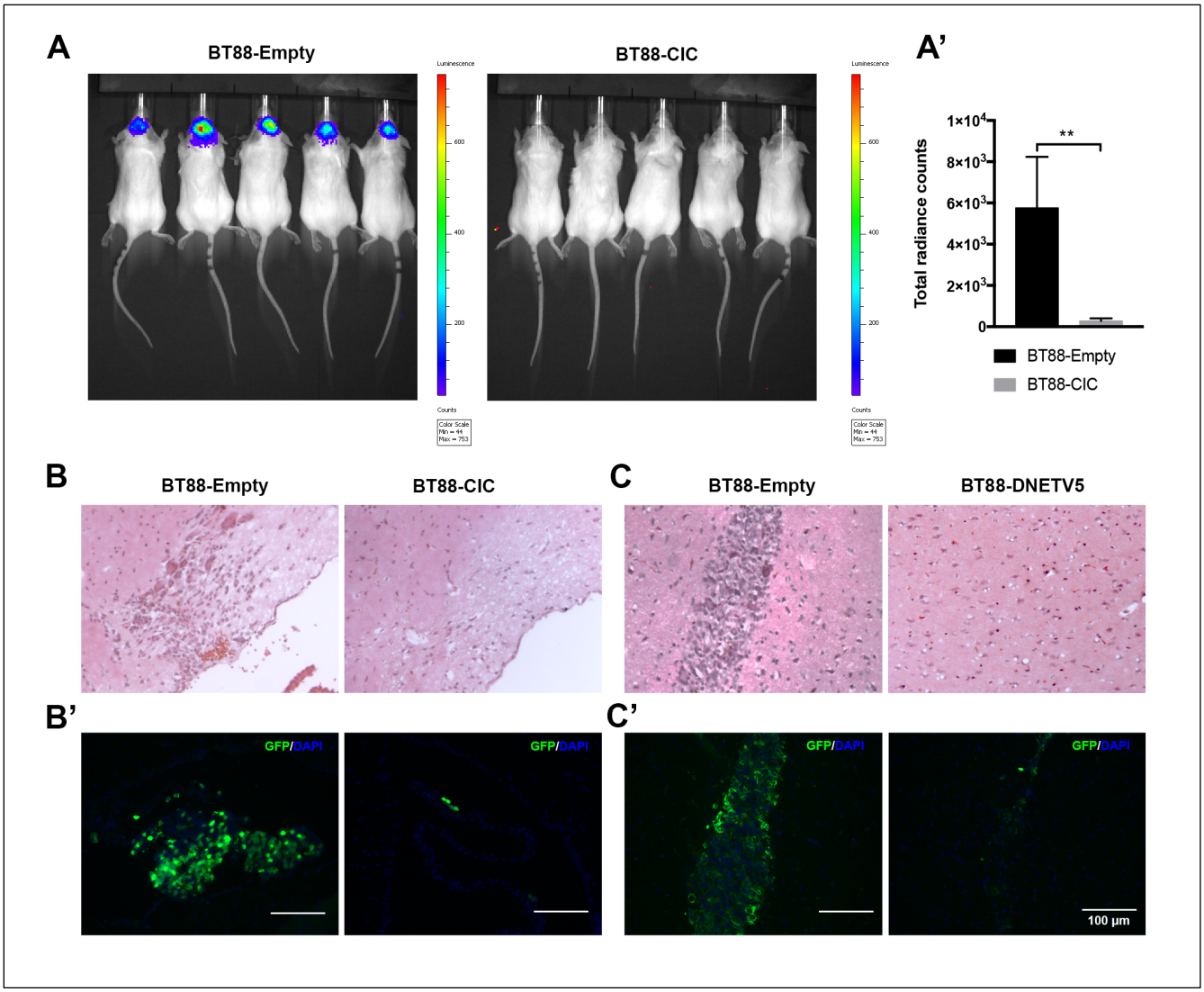

FIGURE 9: Tumorigenicity of ODG cells is reduced by CIC re-expression or ETV5 blockade. (A, A') Bioluminescence imaging of NOD-SCID mice at 6 weeks post-implantation of BT88 oligodendroglioma cells stably transfected with either empty-GFP-luc or CIC-GFP-luc expression vectors. (B,B') Representative images of brain sections from mice implanted with control-GFP-luc BT88 cells or CIC-GFP-luc BT88 cells stained with H&E or GFP. (C,C') Representative images of brain sections from mice implanted with control-GFP BT88 cells or DNETV5-GFP expressing BT88 cells stained with H&E or GFP. Data shown as mean ± SD from 8 mice per group. Statistical analyses by student's t test. **$p<0.01$.